CHAPITRE 3

EFFECTS OF LONG JUMPS, REVERSIBLE AGGREGATION, AND MEYER-NELDEL RULE ON SUBMONOLAYER EPITAXIAL GROWTH

Les sections 3.1 à 3.11 de ce chapitre sont une recopie de l'article de la référence [A. Beausoleil, P. Desjardins, and A. Rochefort, Phys. Rev. E **78**, 021604 (2008)]. Cet article étudie la diffusion sur une surface nominale alors que moins d'une monocouche a été déposée. L'effet des sauts de longue portée et du détachement des atomes de la bordure des îlots est considéré par le biais de simulation KMC. Voici une liste des principales conclusions de cet article.

1) Les sauts de longue portée font augmenter le coefficient de diffusion effectif qui suit alors un comportement supra-Arrhenius.
2) En régime d'agrégation réversible, le détachement des atomes de la bordure des îlots fait croître la densité d'adatomes [1] sur la surface. Comme la densité d'atomes est plus grande, plusieurs petits îlots métastables sont observés sur la surface, de sorte que la distribution de taille des îlots est bimodale.
3) Les points 1) et 2) ont un effet synergique : les atomes qui se détachent de la bordure d'un îlots ont davantage tendance à s'en éloigner si les sauts de longue portée sont possibles, ce qui fait augmenter la densité d'adatomes et d'îlots métastables.
4) La règle de Meyer-Neldel amplifie les points 1), 2) et 3).

3.1 Abstract

We demonstrate, using kinetic Monte Carlo simulations of submonolayer epitaxial growth, that long jumps and reversible aggregation have a major impact on the evolution of island morphologies. Long jumps are responsible for a supra-Arrhenius behavior of the effective diffusion coefficient as the attachment and detachment kinetics give rise to a bimodal island size distribution that depends on temperature and long jump extent limits. As the islands density increases with temperature, the average size of stable islands reaches a maximum before decreasing. We have also observed that the diffusion coefficient cannot be used alone to

1. Un *adatome* est un atome adsorbé sur la surface. Seuls les atomes n'ayant aucun plus proche voisins seront nommés *adatomes* dans cette thèse.

predict the evolution of island sizes and morphologies, the relative rate of each process having a major importance. Our theoretical developments are of direct relevance for materials systems such as Au, Pd, Ag, Cu, Ni, H/Si, H/W(110), Co/Ru and Co/Ru(S), that are known for exhibiting a compensation effect that cannot be contained within experimental uncertainties.

3.2 Introduction

According to the transition state theory (TST), the rate of activation of a diffusion event follows an Arrhenius behavior in the harmonic approximation [15]. That is, if the activation energy is ΔE, the rate is

$$\Gamma = \Gamma_0 e^{-\Delta E/k_B T},$$

where Γ_0 is the attempt frequency or prefactor, T is the temperature, and k_B is the Boltzmann constant.

In 1995, Boisvert *et al.* [192] have shown with an embedded-atom-method molecular-dynamics study that the compensation law or the Meyer-Neldel rule (MNR) could describe self-diffusion rates on Au, Pd, Ag, Cu and Ni. This rule states that the diffusion rate of an event with an activation energy E_i is given by

$$\Gamma_i = \Gamma_{i,0}\left(\Delta E_i\right) e^{-\Delta E_i/k_B T}, \tag{3.1}$$

with the prefactor $\Gamma_{i,0}$ depending on the activation energy as

$$\Gamma_{i,0}(\Delta E_i) = \Gamma_{00} e^{(\Delta E_i/k_B T_{\text{iso}})^{\varepsilon}}. \tag{3.2}$$

Γ_{00} is the constant part of the prefactor, ε is a constant ranging between 1/2 and 1 that depends on the nature of the fundamental excitations [193, 194], and T_{iso} is the isokinetic temperature at which all diffusion events should have an identical rate.

According to the multiple excitation entropy (MEE) model [195], two conditions must be fulfilled to ensure that the MNR applies. That is, the activation energy must be large with respect to the (i) thermal and (ii) elementary excitation energies. Since $k_B T_{\text{iso}}$ is of the order of the elementary excitation energies [195], we can write both conditions as $\Delta E_i \gg k_B T$ and $\Delta E_i \gg k_B T_{\text{iso}}$. The impacts of this law should be more clearly observed in systems at temperatures near T_{iso}. Indeed, as the temperature increases, the rate of high activation energy processes increases much more rapidly than that for low energy processes. At high temperature near T_{iso}, the high energy processes, such as the correlated long jumps in

epitaxial crystal growth, significantly contribute to the total rate of processes. This behavior might considerably affect the surface topography.

Many approaches are possible for understanding and predicting the long jumps phenomenon. Jacobsen *et al.* [196] developed a transition path theory to determine the path of long jumps between second nearest neighbors. They used molecular dynamics to determine that the prefactor is a function of the temperature (proportional to $\sqrt{T}$ in one dimensional diffusion). Montalenti and Ferrando [197] linked long jumps to the potential energy surface and could explain the important differences in the behavior of long jumps observed between (110) surfaces of Cu, Ag and Au although the activation energies of single hops do not show a large variation between the three surfaces. Long jumps can also be linked to surface friction because adatoms exchange energy with the surface. When the friction per unit mass η is small enough, long jumps are more likely. Ferrando *et al.* established what vibrational frequencies and activation energy conditions are required to allow significant long jumps [198]. Assuming a Brownian motion, Chen and Ying [199] solved the equation of movement for an atom subject to friction and reacting to stochastic forces (the Langevin equation) and determined the probability of long jumps for a given friction coefficient, assuming that k_BT is much lower than the potential barrier E_d.

Since long jumps have been shown to have non-negligible probabilities on several surfaces [3, 8–13], their contribution must be considered. For Ag and Au (100) and (111) surfaces, Boisvert and Lewis [200] have shown, using molecular-dynamics simulations within an embedded-atom approach, that correlated long jumps contribute to increase the diffusion coefficient, which then no longer exhibits an Arrhenius behavior. Within a 1D analysis, they find that the diffusion coefficient for long jumps of any extent ℓ for a (100) surface is

$$D^{\mathrm{1D}}_{\ell<\infty} = D^{\mathrm{1D}}_{\ell=1}\left(\frac{1+e^{-\beta}}{1-e^{-\beta}}\right),$$

where $\beta = E_d/k_BT$, with E_d, the diffusion energy barrier. $D^{\mathrm{1D}}_{\ell=1}$ is the 1D diffusion coefficient on the (100) surface when only random walk, that is, between nearest neighbors (NNs), is considered. The diffusion coefficient can be found with the Einstein equation

$$D_{\ell=1} = \lim_{t\to\infty}\frac{\langle R_{\ell=1}(t)^2\rangle}{vt},$$

where $\langle R_{\ell=1}(t)^2\rangle$ is the mean square displacement of an adatom making single hop after a time t, and v is the maximum number of in-plane NNs [e.g., four for a simple cubic (100)

surface]. While the 1D analysis gives some insight on the overall trends, a 2D treatment needs to be considered to completely describe the impact of long jumps on the evolution of island sizes and morphologies during growth. In addition to a greater contribution of long jumps to the total process rates near the isokinetic temperature, the detachment of adatoms, which is less likely to occur at low temperature, can become sufficiently important near T_{iso} to cause a reversible aggregation. Rate equations and kinetic Monte Carlo (KMC) models have been used to study such a regime [201, 202]. Using a KMC model, Ratsch *et al.* [201] reproduce experimental results for Au/Ru(0001) and Ni/Ni(100). They observe an increasing density of islands, which is more precisely related to a larger number of small islands.

For simplicity purposes, the analysis performed to describe the evolution of island sizes and morphologies from experimental or simulated crystal growth data is frequently based on the following assumptions : aggregation is irreversible, diffusion coefficient follows an Arrhenius behavior, the attempt frequency of a diffusion event is constant for every process, and the rate of long jumps is so low with respect to the single hop rate that they can be completely neglected. While such assumptions might be relevant for growth at low temperature, a much different behavior might be observed at high temperatures where the relative difference between the rates of the various processes decrease. This is even more important when the MNR is taken into account.

The present paper focusses on the impact of high energy processes — that may be enhanced by the MNR — on island sizes and morphologies. Our main goal is not to support a universal application of the MNR, but to concentrate on surfaces which have shown compensation effects, such as homoepitaxy on Au, Pd, Ag, Cu and Ni surfaces [192]. Similarly, the growth of Co on Ru(0001) is a system in which the important lateral interactions between adsorbed atoms [203] can lead to important compensation effects [204]. Another example concerns the growth of Co on a vicinal sulfided Ru surface [205], where the diffusion preexponential factor along terraces is more than two orders of magnitude higher than that over the steps while the activation energy of the latter is approximately twice that of the former. Adsorption of H on Si [206–208] and isotopes of H on W(110) [209–211] also reveals compensation effects.

Although it has been shown that other compensation effects can occur with the number of atoms involved in concerted atomic processes [212, 213], we concentrate our work on single atomic motions (single atom diffusion) for simplicity.

We show that when the MNR applies, (i) the supra-Arrhenius behavior predicted for the diffusion coefficient is amplified, and (ii) a bimodal island size distribution is enhanced at high temperatures because of the reversible aggregation regime.

3.3 Model

To observe the impact of high activation energy processes when the temperature increases, we allow long jumps events and detachment in addition to free diffusion, edge diffusion, and diffusion across steps. The relative energy of each process is determined using a simple bond counting model. This allows one to obtain general equations for long jump probabilities and the diffusion coefficient. To observe their individual impact, the MNR, long jumps, and detachment events can be turned off separately.

3.3.1 Long jumps

During the last decade, it has been theoretically [199, 200] and experimentally [214] shown that long jumps have an activation energy that increases linearly, at least in some cases, with the length of the jump. Since we consider long jumps as a combination of single hopping events, the activation energy should increase with the total jump path length. Our model thus forbids backward hops (as part of long jumps) because they require to define an additional energy due to their longer path. This phenomenon should therefore be negligible with respect to straightforward jumps.

We then introduce the notion of *extent*, which is equivalent to the path length when backward hops are forbidden. While the *length* of a jump is the distance between the starting and arrival points, the *extent* of the jump is the minimal number of single hops required to reach the arrival point. On a Cartesian grid within the solid-on-solid (SOS) approximation where the end point is located at coordinates $(\Delta x, \Delta y)$ from the starting point, the *extent* is $\ell = |\Delta x| + |\Delta y|$.

While the starting and arrival points are connected by a single path for single hops, many paths are possible for long jumps. This path multiplicity leads to a different arrival probability for each accessible site. If we note p_i the probability of a jump of extent i following a single path, the global probability pattern for long jumps with an extent limit $\ell_{\max}$ [2] of four atomic units is illustrated in Fig. 3.1. For example, in Fig. 3.1, the dotted arrows correspond to three different paths connecting the same starting and arrival points. Each of these long jump paths have a probability p_3 and the *total* probability for this long jump is $3p_3$ (the single path probability multiplied by the number of different paths). Our model includes such additional entropic contribution, which is not in contradiction with the MEE model [195].

Owing to their dependence on surface friction, Chen *et al.* conclude that indirect long jumps experience more friction and are less likely to occur than direct jumps [215], the former being retrapped more easily. That is, performing a long jump with $|\Delta x|, |\Delta y| < \ell$ should be less favorable than a jump with $|\Delta x| = \ell$ or $|\Delta y| = \ell$. However considering the path followed by long jumps of Ir or W on W(110), Antczak and Ehrlich observed experimentally that the rates of direct and indirect jumps were of the same order [12, 13]. Therefore, to keep our model simple, we define long jumps as a combination of single hops so that p_ℓ is the same for every path of a given jump of extent ℓ.

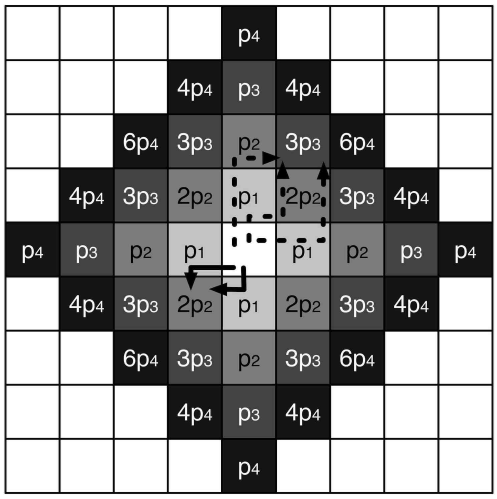

FIGURE 3.1 Jump probabilities pattern for a single adatom in the center of the grid. Each square is an accessible site according to the SOS model. Sites from light gray to black represent sites accessible by jumps of 1, 2, 3 or 4 *extent* atomic units, respectively. p_i is the probability of a long jump of extent i for a single path. The arrows show the path multiplicity for two different sites.

2. The concept of long jump extent limit $\ell_{\max}$ signifies that all jumps with an extent up to $\ell_{\max}$ are considered.

3.3.2 Bond counting

To simplify the theoretical treatment of different processes, we use a simple bond counting model, assuming that energy barriers vary with the number of in-plane NNs before (n_i) and after (n_f) the diffusion event, which is a widely used approach in bond counting KMC simulations [216, 217]. The difference $n_i - n_f$ allows one to favor attachment at high coordination sites (e.g., kinks compared to flat step edges) and to prevent detachment from those sites. We further assume that the energy barriers can be derived from the following equation,

$$\Delta E = n_i E_0 + (n_i - n_f)\, E_\Delta + \ell E_\ell + n_\uparrow E_\uparrow + n_\downarrow E_{\mathrm{ES}}, \tag{3.3}$$

where ℓ is the extent of the jump in atomic units, $n_\uparrow$ is the number of atomic height steps to climb from the initial to the final state, and $n_\downarrow$ is the number of times a step of any height an adatom has to descend to get to the final state. E_0 and E_Δ favor the attachment of adatoms to the islands, E_ℓ is the additional energy needed to increase the extent of the long jump by one atomic unit, $E_\uparrow$ is the energy needed to climb over a monolayer step, and E_{ES} is the Ehrlich-Schwoebel barrier [54, 55]. A minimal energy of $E_{\mathrm{min}} = E_\ell - vE_\Delta$ is associated to every event, where v is the maximum number of NNs in the plane of the atom in the final state [the same value as the one used in Eq. (3.3)] and the energy of diffusion between NNs is $E_d = E_\ell$. This model thus establishes a difference between diffusion on a terrace and diffusion across steps. The attachment of adatoms to islands is favored with respect to the detachment, and the probability of single hopping events is much larger than that for long jumps.

When Eq. (3.3) applies integrally, the reversible aggregation (RA) mode is modeled. We define some other levels of aggregation reversibility following two conditions with respect to the bond counting model parameters. The first condition is that if $n_i > n_i^0$, atoms cannot detach from islands. The second condition is that if $n_i > n_i^0$, attached atoms can only move along island edges. With those conditions, we associate $n_i^0 = 1$ with the first level of reversibility (RA1 mode) and $n_i^0 = 2$ with the second (RA2 mode). In the third, $n_i^0 = 3$, which is the case for the reversible aggregation mode (RA mode) on a Cartesian grid using the SOS approximation. When $n_i^0 = 0$, the irreversible aggregation (IA) mode is modeled. That is, for the IA mode, once an atom is attached to an island, it cannot detach from it. For the RA1 (RA2) mode, atoms surrounded by two (three) NNs or more cannot detach from an island. In the RA mode, atoms must have four NNs to be fixed. The critical island size is not fixed in our study since we treat every island edge in a microstructural way by counting the in-plane

NNs. Therefore, whenever the aggregation mode allows it, atoms can detach from islands of every size.

3.3.3 Long jump probabilities and diffusion coefficient

Our bond counting model allows one to write equations for (i) the relative probability of performing long jumps with respect to single hopping events and (ii) the diffusion coefficient of a single adatom on a flat surface.

For an adatom centered on the Cartesian grid shown in Fig. 3.1, the probability P of presence at $(\Delta x, \Delta y)$ after one diffusion event is

$$P(\Delta x, \Delta y) = \frac{(|\Delta x| + |\Delta y|)!}{|\Delta x|!|\Delta y|!} p_{(|\Delta x|+|\Delta y|)},$$

with p_ℓ [where $\ell = (|\Delta x| + |\Delta y|)$] being the probability of a jump of extent ℓ following a single path as defined earlier.

We can rewrite this equation noting that the right-hand side ratio, which corresponds to the path multiplicity, is a binomial coefficient,

$$P(\Delta x, \Delta y) = \binom{|\Delta x| + |\Delta y|}{|\Delta x|} p_\ell = \binom{\ell}{|\Delta x|} p_\ell.$$

Therefore, the total probability for a long jump of extent ℓ to occur is

$$P_\ell = 4 \sum_{\Delta x=0}^{\ell-1} \binom{\ell}{|\Delta x|} p_\ell = 4\left(2^\ell - 1\right) p_\ell, \tag{3.4}$$

where the fact that

$$P(\Delta x, \Delta y) = P(-\Delta x, -\Delta y) = P(\Delta y, -\Delta x) = P(-\Delta y, \Delta x)$$

was used to simplify the summation in Eq. (3.4).

The normalization of Eq. (3.4) implies that

$$\sum_{\ell=1}^{\ell_{\max}} P_\ell = 1. \tag{3.5}$$

We consider explicitly the MNR as expressed in Eq. (3.2) and assume $\varepsilon = 1$, which represents elementary excitations originating from electrons and optical phonons [193, 194]. Other values of ε can easily be included in the model. For the bond counting model defined by Eq. (3.3), the energy barrier for adatom diffusion over an extent ℓ becomes $\Delta E_\ell = \ell E_\ell$ and the single path probability is

$$p_\ell = k_{\ell \leq \ell_{\max}} \Gamma_\ell = k_{\ell \leq \ell_{\max}} \Gamma_{00} e^{-\alpha \ell},$$

where $\alpha = \frac{E_\ell}{k_B}\left(\frac{1}{T} - \frac{1}{T_{\text{iso}}}\right)$ and $k_{\ell \leq \ell_{\max}}$ is a proportionality constant that depends on the jump extent limit. In this case, Eq. (3.5) allows to define $k_{\ell \leq \ell_{\max}}$:

$$k_{\ell \leq \ell_{\max}} = \begin{cases} \dfrac{1}{4\Gamma_{00}\left(2^{\ell_{\max}+1} - \ell_{\max} - 2\right)} & \text{if } \alpha = 0 \\ \dfrac{2^{\ell_{\max}}}{4\Gamma_{00}\left(2^{\ell_{\max}}\left[\ell_{\max} - 1\right] + 1\right)} & \text{if } \alpha = \ln(2) \\ \dfrac{e^{\alpha}\left(1 - e^{-\alpha}\right)\left(1 - 2e^{-\alpha}\right)}{4\Gamma_{00}\left(1 - e^{-\alpha \ell_{\max}}\left[2^{\ell_{\max}+1}\left\{1 - e^{-\alpha}\right\} - \left\{1 - 2e^{-\alpha}\right\}\right]\right)} & \text{elsewhere,} \end{cases}$$

and

$$k_{\ell < \infty} = \frac{\left(1 - e^{-\alpha}\right)\left(1 - 2e^{-\alpha}\right)}{4\Gamma_{00} e^{-\alpha}}, \quad \text{if } \alpha > \ln(2).$$

Since we restrict the simulation domain of α to be coherent with the MEE model, the condition $\alpha > \ln(2)$ will always be fulfilled and we will omit to recall this condition in the following. We briefly mention that k_∞ is discontinuous for $\alpha \leq \ln(2)$ because the total probability of performing long jumps would increase with the extent of the jump.

We can now write an explicit equation for the total probability of performing a jump of extent ℓ as follows :

$$P_\ell = \frac{\left(2^\ell - 1\right) e^{-\alpha(\ell-1)}\left(1 - e^{-\alpha}\right)\left(1 - 2e^{-\alpha}\right)}{1 - e^{-\alpha \ell_{\max}}\left(2^{\ell_{\max}+1}\left[1 - e^{-\alpha}\right] - \left[1 - 2e^{-\alpha}\right]\right)}, \tag{3.6}$$

$$P_\ell^\infty = \lim_{\ell_{\max} \to \infty} P_\ell = \left(2^\ell - 1\right) \frac{\left(1 - e^{-\alpha}\right)\left(1 - 2e^{-\alpha}\right)}{e^{\alpha(\ell-1)}}. \tag{3.7}$$

Eqs. (3.6) and (3.7) consider the MNR and the path multiplicity of long jumps. However, if such parameters are neglected, the results of Boisvert and Lewis [200], and of Chen and Ying [199], which give $P_\ell^\infty = \left(e^\beta - 1\right) e^{-\ell\beta}$ are reproduced.

When the extent limit $\ell_{\max}$ is finite, the cumulated probability $\delta_{\ell\leq\ell_{\max}}$ of neglected jumps with respect to an infinite extent is an explicit function of $\ell_{\max}$ according to

$$\delta_{\ell\leq\ell_{\max}} \;=\; 1 - \sum_{\ell=1}^{\ell_{\max}} P_\ell^\infty = \frac{\left(2^{\ell_{\max}+1} - 1\right) - \left(2^{\ell_{\max}+1} - 2\right) e^{-\alpha}}{e^{\alpha\ell_{\max}}}. \tag{3.8}$$

The $\delta_{\ell\leq\ell_{\max}}$ parameter allows to determine the difference on the total number of jumps due to the finite extent of jumps. For $\alpha > \ln(2)$, $\delta_{\ell\leq\ell_{\max}}$ decreases with $\ell_{\max}$.

We show in Appendix A (section 3.9) that $D_{\ell\leq\ell_{\max}}$, the diffusion coefficient for a finite jump extent limit, can be written with respect to $D_{\ell=1}$, the diffusion coefficient for single hopping events (random walk). That is,

$$D_{\ell\leq\ell_{\max}} = D_{\ell=1}\nu_{\ell\leq\ell_{\max}}, \tag{3.9}$$

with $D_{\ell=1} = a^2\Gamma_{00}e^{-\alpha}$, and $\nu_{\ell\leq\ell_{\max}}$ a scaling factor that depends on $\ell_{\max}$ and α [see Eqs. (3.14) and (3.16)–(3.20) in Appendix 3.9].

Since the diffusion coefficient is one of the dominant factors that determine the topography of a surface, we evaluate the relative difference between finite and infinite long jump extent limits

$$\Upsilon_{\ell\leq\ell_{\max}} = \frac{D_{\ell<\infty} - D_{\ell\leq\ell_{\max}}}{D_{\ell<\infty}} = \frac{\nu_{\ell<\infty} - \nu_{\ell\leq\ell_{\max}}}{\nu_{\ell<\infty}}. \tag{3.10}$$

We end this section by recalling that our model is two dimensional and considers a path multiplicity. In the absence of a path multiplicity, the diffusion coefficient increases less rapidly with increasing temperature. If only one dimensional diffusion is allowed, we obtain the theoretical results of Boisvert and Lewis [200] with the difference that our model considers explicitly the MNR [3]. We emphasize the fact that the results presented here are valid even for systems where MNR does not apply, except that the evolution of the diffusion

3. If the path multiplicity is not considered, the diffusion coefficient is $D_{\ell<\infty} = D_{\ell=1}\left[\left(1 + e^{-\alpha}\right) / \left(1 - e^{-\alpha}\right)\right]^2$, which should be compared to the theoretical result of Boisvert and Lewis [200] in one dimension in which we apply explicitly the MNR, that is $D_{\ell<\infty} = D_{\ell=1}\left[\left(1 + e^{-\alpha}\right) / \left(1 - e^{-\alpha}\right)\right]$.

coefficient would be closer to the Arrhenius behavior.

This similitude between results considering or not the MNR is due to the fact that there exist temperature and flux conditions which give the same surface evolution in both cases. Those conditions are derived in Appendix 3.10. More precisely, all surface evolutions of simulations that do not consider the MNR are reproduced by simulations that do consider the MNR, but the reverse is not true.

3.4 Methodology and computational details

The theoretical developments of section 3.3.3 and Appendix 3.9 assume a single adatom diffusing on a flat surface. To evaluate the validity of those developments when many adatoms and islands are present on the surface, we use the kinetic Monte Carlo method (KMC) as formulated by Bortz, Kalos and Lebowitz (BKL) [22]. The KMC code allows to simulate the evolution of simple cubic (100) surfaces using the SOS approximation.

In KMC, events are considered as Poisson processes. Therefore, the average time between two successive events is

$$\langle \Delta t \rangle = 1/\mathbf{R}(t), \tag{3.11}$$

where

$$\mathbf{R}(t) = \left[F(t) ab L_x L_y + \sum_i \Gamma_i \right] \tag{3.12}$$

is the total rate of possible events on the surface at a given time. $F(t)$ is the uniform adatom flux (in $1/\mathrm{m}^2\mathrm{s}$) on the surface, $L_x \times L_y$ are the SOS grid dimensions, and a and b are the surface atomic units for a Cartesian grid. Γ_i values are the rates of all possible processes on the surface at a given time. Two uniform random number generators are used in KMC : one integer [218] to choose the location of a deposition event and one real from a Mersenne Twister algorithm [219] to choose the event to perform. The former has a $\delta r < 2.3 \times 10^{-10}$ resolution.

Our simulations were done for a simple cubic (100) surface ($b = a$) with a global flux of $Fa^2 = 0.1$ ML/s and periodic boundary conditions. Simulations were stopped at a coverage of $\theta = 0.2$ ML (total simulation time of $t_{\mathrm{tot}} = \theta/Fab = 2$ s). The size of the simulation grid was $L_x \times L_y = 250 \times 250$. We also make use of normalized coordinates in the simulation by

setting $a = 1$.

In section 3.3.3, we have derived a set of equations for the diffusion coefficient of a single adatom on a flat surface. In the KMC simulations, more than one adatom is diffusing simultaneously and the application of the Einstein equation is not straightforward. In order to evaluate an *effective* diffusion coefficient in the presence of many atoms, we perform a linear regression on adatoms following

$$D' = \frac{\sum_i R(t_i)^2 t_i}{v \sum_i t_i^2}, \tag{3.13}$$

where t_i and $R(t_i)^2$ are respectively, the diffusion time and the square distance of diffusion before the attachment of adatom i. The prime symbol is used to distinguish the effective diffusion coefficient from the theoretical one.

The parameters of the preceding equation are collected as follows. When an adatom is created (by deposition or by detachment from an island), its original position and the simulation time are recorded. Just before the attachment to an island, the total distance of diffusion and the corresponding simulation time are recorded. Therefore, only the contribution of atoms that attach to an island edge or nucleate is compiled to find the effective diffusion coefficient.

While Eq. (3.13) allows to find a good approximation of the real diffusion coefficient, some discrepancies appear in many situations. Among others, let us mention that the compactness and average size of islands, the time the simulation step time takes to stabilize from the beginning of the simulation, the total number of diffusion events, and the average number of steps an adatom takes to attach to an island or to nucleate can all affect D' in such a way that $D' \neq D$. We emphasize on one case relevant to our results. When many islands or adatoms are present on the surface, adatoms that diffuse many times before attaching to an island or nucleating are on average nearer to their starting point than adatoms diffusing on a flat surface since most of those that diffused farther are already part of islands and do not contribute to the effective diffusion coefficient anymore. This results in an effective diffusion coefficient lower than the theoretical diffusion coefficient. Conversely, if most of adatoms that contribute to the effective diffusion coefficient diffuse few before attaching, the effective diffusion coefficient will come nearer to the theoretical diffusion coefficient.

In our KMC simulations, desorption, cluster diffusion, and concerted multicatomic events are not allowed. When an adatom arrives on the surface, it sticks to the arrival point. An adatom surrounded by four in-plane NNs is considered as immobile, and no overhangs are allowed. Processes rates are computed according to the bond counting model of Eq. (3.3) with one of the previously defined aggregation modes, the MNR, when considered, as described by Eqs. (3.1) and (3.2) with $\varepsilon = 1$, and the long jump model and path multiplicity as described by Eq. (3.4) and Fig. 3.1. The numerical parameters of the bond counting model are taken as $E_0 = 0.2$ eV, $E_\ell = 0.3$ eV, $E_\uparrow = E_{\text{ES}} = 0.2$ eV, and $E_\Delta = 0.05$ eV, which are typical experimental activation energies for metals [3, 220–226]. That is, we are modeling metal homoepitaxy for simplicity reasons, although heteroepitaxy might lead to a lower surface friction needed for frequent long jumps. For this reason, we show in Appendix 3.10 that the activation energies can be shifted without changing the global trends.

In order to compare simulations that apply the MNR with others that do not, we need to fix a simulation parameter (other than the flux and the total coverage) that will be the same in every simulation. Since the most frequent process in our simulations that considered the MNR is the free diffusion one ($n_i = n_f = n_\uparrow = n_\downarrow = 0$ and $\ell = 1$), we gave an equivalent prefactor to this process in all simulations. That is, for a same simulation temperature, the rate of the free diffusion process will always be the same whether the MNR applies or not. When the MNR does not apply, the prefactor in Eq. (3.1) does not depend on the activation energy and the common prefactor of all processes is therefore $\Gamma_0 = \Gamma_{00} e^{-E_\ell / k_B T_{\text{iso}}}$.

We set $\Gamma_{00} = 10^5$ s^{-1} to cover many orders of magnitude in the range of prefactors when the MNR applies, as can be observed in many systems [195]. Moreover, T_{iso} is fixed to 348.13 K. We recall the conditions that warrant that the MNR applies according to the MEE model : the activation energies are much larger than (i) $k_B T_{\text{iso}}$, and (ii) $k_B T$. Moreover, the MNR often fails above T_{iso} [195] so that we set $T < T_{\text{iso}}$. To fulfill those conditions, the highest simulation temperature is fixed to $T_{\max} = 280$ K. This also ensures that the isokinetic temperature is near the experimental range as frequently observed [195].

We draw the reader's attention to the fact that the value of T_{iso} is somewhat arbitrary since few data are available in the literature. Moreover, our simulations are set for $E_d/k_B T \geq E_d/k_B T_{\max} = 12.4$, while long jumps and other concerted motions should be non-negligible for $E_d/k_B T \lesssim 4$ [152]. However, as shown in Appendix 3.10, our results can be transposed to almost any T_{iso} value without loosing global trends. That is, the temperature values we used are not absolute and should always be considered relatively to T_{iso}. For

instance, Appendix 3.10 shows that multiplying T_{iso} by 10 results in values of E_d/k_BT ranging from 3.4 to 4.9 that give the same surface morphology as those with $E_d/k_BT \geq 12.4$.

A complete KMC treatment would require a simulation of jump extents up to infinity. However, such a treatment is far from being computationally realistic. A cutoff must be made in the long jump extent limit. To do so, we recall that the highest simulated temperature is $T = 280$ K. This allows us to give in Table 3.1 the relative difference between finite and infinite long jump extent limits on the number of jumps and the diffusion coefficient according to Eqs. (3.8) and (3.10). We clearly see that considering only single hops can lead to a significant underestimation of the overall diffusion coefficient, especially at higher temperatures. Table 3.1 also reveals that using a jump extent limit of four atomic units is sufficient to ensure that the total number of jumps and the overall diffusion coefficient are within 1.5 % of their saturation values for an infinite extent limit for the temperatures considered in this study. We therefore limit the jump extent to four atomic units in our simulations.

TABLEAU 3.1 Difference between finite and infinite long jump extent limits ($\ell_{\max}$) for the total number of jumps ($\delta_{\ell\leq\ell_{\max}}$) and the diffusion coefficient ($\Upsilon_{\ell\leq\ell_{\max}}$). These values are derived from Eqs. (3.8) and (3.10).

	$T = 250$ K		$T = 265$ K		$T = 274$ K		$T = 280$ K	
$\ell_{\max}$	$\delta_{\ell\leq\ell_{\max}}$ (%)	$\Upsilon_{\ell\leq\ell_{\max}}$ (%)	$\delta_{\ell\leq\ell_{\max}}$ (%)	$\Upsilon_{\ell\leq\ell_{\max}}$ (%)	$\delta_{\ell\leq\ell_{\max}}$ (%)	$\Upsilon_{\ell\leq\ell_{\max}}$ (%)	$\delta_{\ell\leq\ell_{\max}}$ (%)	$\Upsilon_{\ell\leq\ell_{\max}}$ (%)
1	5.84	9.56	12.65	20.19	19.16	29.84	24.78	37.74
2	0.27	1.13	1.27	4.86	2.95	10.31	4.98	16.12
3	0.01	0.09	0.12	0.83	0.42	2.66	0.93	5.35
4	0.00	0.01	0.01	0.12	0.06	0.58	0.17	1.51
5	0.00	0.00	0.00	0.01	0.01	0.11	0.03	0.39

3.5 Results

Throughout this section, we present island size distributions and average island sizes in the submonolayer regime to evaluate the impact of the aggregation mode, the long jumps and the MNR. We do not make use of scaling laws of the form

$$n_{\text{ad}} \sim \theta^{1/(i+2)} \left(\frac{F}{D}\right)^{i/(i+2)} e^{E_c(i)/(i+2)k_BT},$$

where n_{ad} is the density of islands, i is the critical size of islands and $E_c(i)$ is the cohesion energy of islands of size i, because such laws are relevant only if one of the two following